THE CNOIDAL METHOD WITH APPLICATION TO SONIC COMPOSITES

Ligia MUNTEANU[1], Valerica MOŞNEGUŢU[2], Veturia CHIROIU[3], Ruxandra ILIE[4]

The sound attenuation in a sonic composite is studied by using the cnoidal method combined with the features of the piezoceramic theory. The solutions of nonlinear equations which govern the behavior of the sonic composites are written as a sum of a linear and nonlinear cnoidal functions. A sonic composite consists of an array of acoustic scatterers embedded in an epoxy matrix. Acoustic scatterers are piezoceramic hollow spheres made from functionally graded materials - the Reddy graded hollow spheres. The influence of the Reddy gradient index on the full band-gap size is studied using the cnoidal representations of the solutions.

Keywords: cnoidal method, sonic composites, piezoceramic scatterers, full band-gap.

1. Cnoidal method

The mathematical and physical structure of the inverse scattering transform solutions has been extensively studied in both one and two dimensions [1-4]. The theta-function representation of the solutions is describable as a linear superposition of Jacobi elliptic functions and additional terms, which include nonlinear interactions among them. The cnoidal method is a generalization of the Fourier series with the cnoidal functions as the fundamental basis function [5]. This is because the cnoidal functions are much richer than the trigonometric or hyperbolic functions, that is, the modulus m of the cnoidal function, $0 \le m \le 1$, can be varied to obtain a sine or cosine function $(m \cong 0)$, a Stokes function $(m \cong 0.5)$ or a solitonic function, sech or tanh $(m \cong 1)$.

Legendre was the first who works with Jacobi elliptic integrals of the first and the second kinds $E(z)$ and $F(z)$ respectively, being followed by Abel (1802–1829) and Jacobi (1804–1851). Jacobi inspired by Gauss, discovered in 1820 that

[1] Institute of Solid Mechanics, Romanian Academy, Bucharest, Romania, ligia_munteanu@hotmail.com
[2] Institute of Solid Mechanics, Romanian Academy, Bucharest, Romania, valeriam73@yahoo.com
[3] Institute of Solid Mechanics, Romanian Academy, Bucharest, Romania, veturiachiroiu@yahoo.com
[4] Technical University of Civil Engineering, Bucharest, Romania, rux_i@yahoo.com

the inverse of $F(z)$ is an elliptical double-periodic integral $F^{-1}(\omega)=\mathrm{sn}(\omega)$ Jacobi compares the integral

$$v=\int_0^{\varphi}\frac{\mathrm{d}\theta}{(1-m\sin^2\theta)^{1/2}} \tag{1}$$

where $0\le m\le 1$, to the elementary integral

$$w=\int_0^{\varphi}\frac{\mathrm{d}t}{(1-t^2)^{1/2}} \tag{2}$$

and observed that (2) defines the inverse of the trigonometric function sin if we use the notations $t=\sin\theta$ and $\psi=\sin w$. He defines a new pair of inverse functions from (1)

$$\mathrm{sn}\,v=\sin\varphi,\ \mathrm{cn}\,v=\cos\varphi. \tag{3}$$

These are two of the Jacobi elliptic functions, usually written $\mathrm{sn}(v,m)$ and $\mathrm{cn}(v,m)$ to denote the dependence on the parameter m. The angle φ is called the amplitude $\varphi=\mathrm{am}\,u$. We also define the Jacobi elliptic function $\mathrm{dn}v=(1-m\sin^2\varphi)^{1/2}$. For $m=0$, we have

$$\mathrm{cn}(v,0)=\cos\varphi=\cos v,\ \mathrm{sn}(v,0)=\sin\varphi=\sin v,\ \mathrm{dn}(v,0)=1, \tag{4}$$

and for $m=1$

$$\mathrm{cn}(v,1)=\mathrm{sech}v,\ \mathrm{sn}(v,1)=\tanh v,\ \mathrm{dn}(v,1)=\mathrm{sech}v. \tag{5}$$

The functions $\mathrm{sn}\,v$ and $\mathrm{cn}\,v$ are periodic functions with the period $\int_0^{2\pi}\frac{\mathrm{d}\theta}{(1-m\sin^2\theta)^{1/2}}=4\int_0^{\pi/2}\frac{\mathrm{d}\theta}{(1-m\sin^2\theta)^{1/2}}$. The later integral is the complete elliptic integral of the first kind

$$K(m)=\int_0^{\pi/2}\frac{\mathrm{d}\theta}{(1-m\sin^2\theta)^{1/2}}. \tag{6}$$

The period of the function $\mathrm{dn}\,v$ is $2K$. For $m=0$ we have $K(0)=\pi/2$. For increasing of m, $K(m)$ increases monotonically $K(m)\approx\frac{1}{2}\log\frac{16}{1-m}$. Thus, this periodicity of $\mathrm{sn}\,(v,1)$ and $\mathrm{cn}\,(v,1)=\mathrm{sech}v$ is lost for $m=1$, so $K(m)\to\infty$.

Now, let us consider the Weierstrass function $\wp(t)$ which verifies the equation

$$\dot{\wp}^2=4\wp^3-g_2\wp-g_3. \tag{7}$$

If e_1,e_2,e_3 are real roots of the equation $4y^3-g_2y-g_3=0$ with $e_1>e_2>e_3$, then (7) can be written as

$$\dot{\wp}^2 = 4(\wp - e_1)(\wp - e_2)(\wp - e_3), \tag{8}$$

with $g_2 = 2(e_1^2 + e_2^2 + e_3^2)$, $g_3 = 4e_1 e_2 e_3$, $e_1 + e_2 + e_3 = 0$. Introducing $\Delta = g_2^3 - 27g_3^2$ when $\Delta > 0$, equation (9) admits the elliptic Weierstrass function as a particular solution, which is reducing in this case to the Jacobi elliptic function cn

$$\wp(t + \delta'; g_2, g_3) = e_2 - (e_2 - e_3)\mathrm{cn}^2(\sqrt{e_1 - e_3}\, t + \delta') \tag{9}$$

where δ' is an arbitrary real constant. If we impose initial conditions

$$\wp(0) = \theta_0, \quad \wp'(0) = \theta_{p0}, \tag{10}$$

then a linear superposition of cnoidal functions (9) is also a solution for (7)

$$\theta_{lin} = 2\sum_{k=0}^{n} \alpha_k \mathrm{cn}^2[\omega_k t; m_k], \tag{11}$$

where the angular frequencies ω_k, and amplitudes α_k depend on θ_0, θ_{p0}.

When $\Delta < 0$ the solution of (8) is

$$\wp = e_2 + H_2 \frac{1 + \mathrm{cn}(2t\sqrt{H_2} + \delta')}{1 - \mathrm{cn}(2t\sqrt{H_2} + \delta')},$$

with $m = \frac{1}{2} - \frac{3e_2}{4H_2}$, $H_2 = 3e_2^2 - \frac{g_2}{4}$.

Consider now a generalized Weierstrass equation with a polynomial of n degree in $\theta(t)$

$$\dot{\theta}^2 = P_n(\theta). \tag{12}$$

The functional form of solutions of (12) is determined by the zeros of the right-hand side polynomial.

Osborne [1] discussed this method for integrable nonlinear equations that have periodic boundary conditions, and Munteanu and Donescu [5] have extended this method to nonlinear partial differential equations that can be reduced to Weierstrass equations of the type (12).

The general solution of (12) may be written in the terms of the *theta function* representation [6]

$$\theta(x,t) = \frac{2}{\lambda}\frac{\mathrm{d}^2}{\mathrm{dx}^2}\log\Theta_n(\eta_1, \eta_2, ..., \eta_n), \tag{13}$$

where $\lambda = \alpha / 6\beta$, and Θ is the *theta function* defined as

$$\Theta_n(\eta_1, \eta_2, ..., \eta_n) = \sum_{M \in (-\infty, \infty)} \exp\left(\mathrm{i}\sum_{i=1}^{n} M_i \eta_i + \frac{1}{2}\sum_{i,j=1}^{n} M_i B_{ij} M_j\right), \tag{14}$$

with n the number of degrees of freedom for a particular solution of the KdV equation, and

$$\eta_j = k_j x - \omega_j t + \phi_j, \; 1 \le j \le N. \tag{15}$$

In (15), k_j are the wave numbers, the ω_j are the frequencies and the ϕ_j are the phases. Let us introduce the vectors of wave numbers, frequencies and constant phases

$$\begin{aligned} &k=[k_1,k_2,...,k_n],\ \omega=[\omega_1,\omega_2,...,\omega_n],\\ &\phi=[\phi_1,\phi_2...,\phi_n],\ \eta=[\eta_1,\eta_2,...,\eta_n]. \end{aligned} \tag{16}$$

The vector η can be written as $\eta = kx-\omega t+\phi$.

Also, we can write $M\eta = Kx-\Omega t+\Phi$, $M=[M_1,M_2,...,M_n]$, $K=Mk$, $\Omega = M\omega$, $\Phi = M\phi$.

The integer components in M are the integer indices in (17). The matrix B can be decomposed in a diagonal matrix D and an off-diagonal matrix O, that is

$$B = D+O. \tag{17}$$

THEOREM [5]. *The solution* $\theta(x,t)$ *of equation* (12) *can be written as*

$$\theta(x,t)=\frac{2}{\lambda}\frac{\partial^2}{\partial x^2}\log\Theta_n(\eta)=\theta_{lin}(\eta)+\theta_{int}(\eta), \tag{18}$$

where θ_{lin} *represents a linear superposition of cnoidal functions*

$$\theta_{lin}(\eta)=\frac{2}{\lambda}\frac{\partial^2}{\partial x^2}\log G(\eta),\qquad G(\eta)=\sum_M \exp\left(\mathrm{i}M\eta+\frac{1}{2}M^TDM\right),$$

and θ_{int} *represents a nonlinear interaction among the cnoidal functions*

$$\begin{aligned} \theta_{\mathrm{int}}(\eta)&=2\frac{\partial^2}{\partial t^2}\log\left(1+\frac{F(\eta,C)}{G(\eta)}\right),\\ \theta_{\mathrm{int}}(\eta)&=2\frac{\partial^2}{\partial t^2}\log\left(1+\frac{F(\eta,C)}{G(\eta)}\right), \end{aligned} \tag{19}$$

$$C=\exp\left(\frac{1}{2}M^TOM\right)-1. \tag{20}$$

Consider now a nonlinear system of equations that govern the motion of a dynamical system

$$\frac{\mathrm{d}\theta_i}{\mathrm{d}t}=F_i(\theta_1,\theta_2,...,\theta_n),\quad i=1,...,n,\quad n\geq 3, \tag{21}$$

with $x\in\mathrm{R}^n$, $t\in[0,T]$, $T\in\mathrm{R}$, where F may be of the form

$$F_i = \sum_{p=1}^{n} a_{ip}\theta_p + \sum_{p,q=1}^{n} b_{ipq}\theta_p\theta_q + \sum_{p,q,r=1}^{n} c_{ipqr}\theta_p\theta_q\theta_r + \\ + \sum_{p,q,r,l=1}^{n} d_{ipqrl}\theta_p\theta_q\theta_r\theta_l + \sum_{p,q,r,l,m=1}^{n} e_{ipqrlm}\theta_p\theta_q\theta_r\theta_l\theta_m + \ldots, \tag{22}$$

with $i = 1, 2, ..., n$, and $a, b, c...$ constants.

The system of equations has the remarkable property that it can be reduced to Weierstrass equations of the type (12). In the following, we present the cnoidal method, suitable to be used for equations of the form (21). To simplify the presentation, let us omit the index i and note the solution by $\theta(t)$.

We introduce the function transformation

$$\theta = 2\frac{\mathrm{d}^2}{\mathrm{d}t^2}\log\Theta_n(t), \tag{23}$$

where the theta function $\Theta_n(t)$ are defined as

$$\begin{aligned}
&\Theta_1 = 1 + \exp(\mathrm{i}\omega_1 t + B_{11}),\\
&\Theta_2 = 1 + \exp(\mathrm{i}\omega_1 t + B_{11}) + \exp(\mathrm{i}\omega_2 t + B_{22}) + \exp(\omega_1 + \omega_2 + B_{12}),\\
&\Theta_3 = 1 + \exp(\mathrm{i}\omega_1 t + B_{11}) + \exp(\mathrm{i}\omega_2 t + B_{22}) + \exp(\mathrm{i}\omega_3 t + B_{33}) +\\
&+ \exp(\omega_1 + \omega_2 + B_{12}) + \exp(\omega_1 + \omega_3 + B_{13}) + \exp(\omega_2 + \omega_3 + B_{23}) +\\
&+ \exp(\omega_1 + \omega_2 + \omega_3 + B_{12} + B_{13} + B_{23}),
\end{aligned} \tag{24}$$

and

$$\Theta_n = \sum_{M\in(-\infty,\infty)} \exp(\mathrm{i}\sum_{i=1}^{n} M_i\omega_i t + \frac{1}{2}\sum_{i<j}^{n} B_{ij}M_iM_j), \tag{25}$$

$$\exp B_{ij} = \left(\frac{\omega_i - \omega_j}{\omega_i + \omega_j}\right)^2, \exp B_{ii} = \omega_i^2. \tag{26}$$

Further, consider (17) and write the solution (23) under the form

$$\theta(t) = 2\frac{\partial^2}{\partial t^2}\log\Theta_n(\eta) = \theta_{lin}(\eta) + \theta_{int}(\eta), \tag{27}$$

for $\eta = -\omega t + \phi$. The first term θ_{lin} represents, as above, a linear superposition of cnoidal waves. Indeed, after a little manipulation and algebraic calculus, (23) gives

$$\theta_{lin} = \sum_{l=1}^{n}\alpha_l\left[\frac{2\pi}{K_l\sqrt{m_l}}\sum_{k=0}^{\infty}\left(\frac{q_l^{k+1/2}}{1+q_l^{2k+1}}\cos(2k+1)\frac{\pi\omega_l t}{2K_l}\right)^2\right]. \tag{28}$$

In (28) we recognize the expression [7, 8]

$$\theta_{lin} = \sum_{l=1}^{n} \alpha_l \mathrm{cn}^2[\omega_l t; m_l], \tag{29}$$

with

$$q = \exp\left(-\pi \frac{K'}{K}\right), K = K(m) + \int_0^{\pi/2} \frac{\mathrm{d}u}{\sqrt{1 - m\sin^2 u}}, K'(m_1) = K(m), \quad m + m_1 = 1.$$

The second term θ_{int} represents a nonlinear superposition or interaction among cnoidal waves. We write this term as

$$2\frac{\mathrm{d}^2}{\mathrm{d}t^2}\log\left(1 + \frac{F(t)}{G(t)}\right) \approx \frac{\beta_k \mathrm{cn}^2(\omega t, m_k)}{1 + \gamma_k \mathrm{cn}^2(\omega t, m_k)}. \tag{30}$$

If m_k take the values 0 or 1, the relation (30) is directly verified. For $0 \le m_k \le 1$, the relation is numerically verified with an error of $|e| \le 5 \times 10^{-7}$. Consequently, we have

$$\theta_{int}(x,t) = \frac{\sum_{k=0}^{n} \beta_k \mathrm{cn}^2[\omega_k t; m_k]}{1 + \sum_{k=0}^{n} \lambda_k \mathrm{cn}^2[\omega_k t; m_k]}. \tag{31}$$

As a result, the cnoidal method yields to solutions consisting of a linear superposition and a nonlinear superposition of cnoidal functions.

2. Formulation of the problem

In this paper we solve the nonlinear equations of a sonic composite by using the cnoidal method. The task of our study is to analyze the influence of the Reddy gradient index on the full band-gap size. The proposed task is investigated by using the theory of piezoelectrics coupled with the cnoidal method.

A sonic composite is a finite size periodic array composed of scatterers embedded in a homogeneous material [9-11]. A sonic composite exhibits the full band-gaps, where the sound is not allowed to propagate due to complete reflections. The band-gaps are defined by well-known Bragg reflections which occur at different frequencies inverse proportional to the central distance between two scatterers. If the band-gaps are not wide enough, their frequency ranges do not overlap. These band-gaps can overlap due to reflections on the surface of scatterers as well as due to wave propagation inside them. Then, any wave is reflected completely from this periodic array of acoustic scatterers in the frequency range where all the band-gaps for the different periodical directions overlap. This is the fundamental mechanism for the formation of a full band-gap which is required for photonic and sonic crystals. The complete reflection on the boundaries of scatterers is due to the full band-gap property itself independent of

the incident angle. The evanescent field distributes across the boundary of the waveguide into the surrounding composite by several times the central distance between two scatterers.

The scatterers are made from functionally graded materials with radial polarization which support the Reddy law [12, 13]. For a single sphere made from a functionally graded material, the free vibration problem was analyzed in [14-16].

Absorption of sound is governed by visco-thermal effects. The sound absorption can be understood by conversion of the wave energy into heat. In sonic composites, the generation of full band-gaps creates sound blocking mechanisms only by full reflection of sound. In this way the waves are prevented to penetrate through material. The full band-gap generation is caused by evanescent modes and will not easily lead to broadband absorption of sound. The present paper is not considering the visco-thermal effects.

Let us consider a composite thin plate consisting of an array of acoustic scatterers embedded in an epoxy matrix [9]. The acoustic scatterers are hollow spheres made from isotropic piezoelectric ceramic, while the matrix is made from isotropic epoxy resin (Fig. 1). The sonic plate consists of 72 local resonators of diameter a. A rectangular coordinate system $Ox_1x_2x_3$ is employed. The origin of the coordinate system $Ox_1x_2x_3$ is located at the left end, in the middle plane of the sample, with the axis Ox_1 in-plane and normal to the layers and the axis Ox_3 out-plane and normal to the plate. The length of the plate is L, its width is d, while the diameter of the hollow sphere is a and its thickness is $e > a$.

For sonic crystals consisting of local resonators, we reduce the total number of time steps in the simulation since the attenuation is mostly due to local effects within the scatterers. In order to avoid unphysical reflections from the boundaries of the specimen, we have implemented the absorbing boundary conditions in the x_1-direction, at $x_1 = 0$ and $x_1 = L$. A transducer and a receiver are located at $x_1 = b$ and $x_1 = L - b$, respectively. The role of the transducer is to inject into the plate the plane monochromatic waves propagating in the x_1-direction.

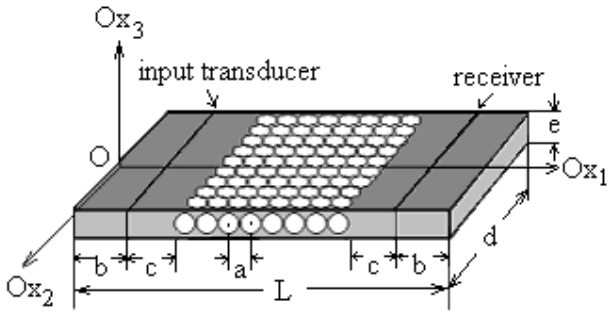

Fig. 1. Sketch of the sonic plate.

The displacements are registered at both sides of the plate. The sound attenuation coefficient is obtained from the ratio of the displacements at the receiver and at the input transducer. The basic equations of 3D spherically isotropic piezoelasticity for a sphere are [9]

$$
\begin{aligned}
&r\sigma_{\theta\theta} = C_{11}S_{\theta\theta} + C_{12}S_{\varphi\varphi} + C_{13}S_{rr} + f_{31}r\phi_r,\\
&r\sigma_{\varphi\varphi} = C_{12}S_{\theta\theta} + C_{11}S_{\varphi\varphi} + C_{13}S_{rr} + f_{31}r\phi_{,r},\\
&r\sigma_{rr} = C_{13}S_{\theta\theta} + C_{13}S_{\varphi\varphi} + C_{33}S_{rr} + f_{33}r\phi_{,r},\\
&r\sigma_{r\theta} = 2C_{44}S_{r\theta} + f_{15}\phi_{,\theta},\ r\sigma_{r\varphi} = 2C_{44}S_{r\varphi} + f_{15}\csc\theta\phi_{,\varphi},\\
&r\sigma_{\theta\varphi} = 2C_{66}S_{\theta\varphi},\ rD_\theta = 2C_{15}S_{r\theta} - \zeta_{11}\phi_{,\theta},\\
&rD_\varphi = 2f_{15}S_{r\varphi} - \zeta_{11}\csc\theta\phi_{,\varphi},\\
&rD_r = f_{31}S_{\theta\theta} + f_{31}S_{\varphi\varphi} + f_{33}S_{rr} - \zeta_{33}r\phi_{,r},
\end{aligned}
\tag{32}
$$

where σ_{ij} is the stress tensor, ϕ is the electric potential, D_i is the electric displacement vector, C_{ij} are the elastic constants, $C_{66} = (C_{11} - C_{12})/2$, f_{ij} are the piezoelectric constants f_{ij}, ζ_{ij} are the dielectric constants, and $i = r, \theta, \varphi$. The elastic, piezoelectric and dielectric constants are arbitrary functions of the radial coordinate r. On denoting the components of the strain tensor and displacement vector by ε_{ij} and u_i, $i = r, \theta, \varphi$, respectively, the quantities S_{ij} related to the strain tensor ε_{ij} are defined as

$$
\begin{aligned}
&S_{rr} = r\varepsilon_{rr} = ru_{r,r},\ S_{\theta\theta} = r\varepsilon_{\theta\theta} = u_{\theta,\theta} + u_r,\\
&S_{\varphi\varphi} = r\varepsilon_{\varphi\varphi} = \csc\theta u_{\varphi,\varphi} + u_r + u_\theta\cot\theta,\\
&2S_{r\theta} = 2r\varepsilon_{r\theta} = u_{r,\theta} + ru_{\theta,r} - u_\theta,\\
&2S_{r\varphi} = 2r\varepsilon_{r\varphi} = \csc\theta u_{r,\varphi} + ru_{\varphi,r} - u_\varphi,\\
&2S_{\theta\varphi} = 2r\varepsilon_{\theta\varphi} = \csc\theta u_{\theta,\varphi} + u_{\varphi,\theta} - u_\varphi\cot\theta.
\end{aligned}
\tag{33}
$$

Denoting the density of the material by ρ, which is assumed to be an arbitrary function of r, the equations of motion become

$$\begin{aligned}
&(r\sigma_{r\theta})_{,r} + \csc\theta(\sigma_{\theta\varphi})_{,\varphi} + (\sigma_{\theta\theta})_{,\theta} + 2\sigma_{r\theta} + (\sigma_{\theta\theta} - \sigma_{\varphi\varphi})\cot\theta = \rho r\ddot{u}_{\theta},\\
&(r\sigma_{r\varphi})_{,r} + \csc\theta(\sigma_{\varphi\varphi})_{,\varphi} + (\sigma_{\theta\varphi})_{,\theta} + 2\sigma_{r\varphi} + 2\sigma_{\theta\varphi}\cot\theta = \rho r\ddot{u}_{\varphi},\\
&\sigma_{rr,r} + \csc\theta\sigma_{r\varphi,\varphi} + \sigma_{r\theta,\theta} + \sigma_{rr} - \sigma_{\theta\theta} - \sigma_{\varphi\varphi} + \sigma_{r\theta}\cot\theta = \rho r\ddot{u}_{r}.
\end{aligned} \tag{34}$$

The charge equation of electrostatics is given by

$$D_{r,r} + D_r + \csc\theta(D_\theta \sin\theta)_{,\theta} + \csc\theta D_{\varphi,\varphi} = 0. \tag{35}$$

The Chen functions F, G and w, and the stress functions Σ_1, Σ_2 are defined as [15]

$$u_\theta = -\csc\theta F_{,\varphi} - G_{,\theta},\ \ u_\varphi = F_{,\theta} - \csc\theta G_{,\varphi},\ \ u_r = w,$$
$$\sigma_{r\theta} = -\csc\theta\sigma_{1,\varphi} - \sigma_{2,\theta},\ \ \sigma_{r\varphi} = \sigma_{1,\theta} - \csc\theta\sigma_{2,\varphi}.$$

are used in order to simplify equations (32)-(35). Therefore, these equations can be separated into two independent sets of equations

$$rA_{,r} = VA,\ rB_{,r} = PB, \tag{36}$$

where

$$B = [r\sigma_{rr}, \Sigma_2, G, w, rD_r, \phi]^T,\quad V = \begin{bmatrix} -2 & -C_{66}(\nabla^2 + 2) + r^2\rho\dfrac{\partial^2}{\partial t^2} \\ C_{44}^{-1} & 1 \end{bmatrix},$$

and $\nabla^2 = \dfrac{\partial^2}{\partial\theta^2} + \cot\theta\dfrac{\partial}{\partial\theta} + \csc^2\theta\dfrac{\partial^2}{\partial\varphi^2}$.

It should be noted that the first equation (36) is related to two state variables, namely $A = [\Sigma_1, F]^T$, while the second set of equations (36) are related to the following six state variables $B = [r\sigma_{rr}, \Sigma_2, G, w, rD_r, \phi]^T$.

The nonzero components of the matrix P are given by

$$P_{11} = 2\beta - 1,\ P_{12} = \nabla^2,\ \ P_{13} = k_1\nabla^2,\ P_{14} = -2k_1 + r^2\rho\frac{\partial^2}{\partial t^2},$$

$$P_{15} = 2P_{25} = -P_{64} = 2\gamma,\ P_{21} = \beta,\ P_{22} = -2,\ \ P_{23} = k_2\nabla^2 - 2C_{66} + r^2\rho\frac{\partial^2}{\partial t^2},$$
$$P_{24} = -k_1,\quad P_{32} = C_{44}^{-1},\quad P_{33} = P_{34} = -P_{55} = 1,\quad P_{36} = C_{44}^{-1}f_{15},\quad P_{41} = \alpha^{-1}\zeta_{33},$$
$$P_{43} = \beta\nabla^2,\quad P_{44} = -2\beta,\quad P_{45} = \alpha^{-1}f_{33},\quad P_{52} = C_{44}^{-2}f_{15}\nabla^2,\quad P_{56} = k_3\nabla^2,$$
$$P_{61} = \alpha^{-1}f_{33},\ P_{63} = \gamma\nabla^2,\ P_{65} = -\alpha^{-1}C_{33},$$

where

$$\alpha = C_{33}\zeta_{33} + f_{33}^2,\ \ \beta = \alpha^{-1}(C_{13}\zeta_{33} + f_{31}f_{33}),\ \gamma = \alpha^{-1}(C_{13}f_{33} - C_{33}f_{31}),$$

$k_1 = 2(C_{13}\beta + f_{31}\gamma) - (C_{11} + C_{12})$, $k_2 = 0.5k_1 - C_{66}$, $k_3 = \zeta_{11} + f_{15}^2 C_{44}^{-1}$.

The scatterers are made from functionally graded materials with radial polarization, which support the Reddy law given by [12, 13]

$$M = M_p \mu^\lambda + M_z (1 - \mu^\lambda), \tag{37}$$

where $\mu = (b - r)/(b - a)$, λ is the inhomogeneity parameter or gradient index, M_p and M_z are material constants of two materials, namely PZT-4 and ZnO [17, 18]. The case $\lambda = 0$ corresponds to a homogeneous PZT-4 hollow sphere and $\lambda \to \infty$, to a homogeneous ZnO hollow sphere.

The constitutive equations for epoxy-resin material are given by

$$t_{ij} = \lambda^e \varepsilon_{kk} \delta_{ij} + 2\mu^e \varepsilon_{ij} + A^e \varepsilon_{il} \varepsilon_{jl} + 3B^e \varepsilon_{kk} \varepsilon_{ij} + C^e \varepsilon_{kk}^2 \delta_{ij} \tag{38}$$

where t_{ij} is the stress tensor, ε_{ij} is the strain tensor, λ^e and μ^e are the Lamé elastic constants, and A^e, B^e and C^e are the second-order elastic constants. The motion equations can be recast as

$$\rho^e \ddot{u}_i = t_{ij.j}, \tag{39}$$

where ρ^e is density of the epoxy material and u is the displacement vector.

At the interfaces between the hollow spheres and the matrix, sharp periodic boundary conditions for the displacement and traction vectors are added. After algebraically manipulations, the set of equations (36-39) are reducing to equations of the form (21) and (22).

3. Results

Consider a plate with the length $L = 18\text{cm}$ and width $d = 11\text{cm}$, while the diameter of the hollow sphere and its thickness are $a = 10.5\text{mm}$ and $e = 12\text{mm}$, respectively. The numerical results are carried out for the following constants:

for PZT-4

$C_{11} = 13.9 \times 10^{10}\,\text{N/m}^2$, $C_{12} = 7.8 \times 10^{10}\,\text{N/m}^2$, $C_{13} = 7.4 \times 10^{10}\,\text{N/m}^2$,

$C_{33} = 11.5 \times 10^{10}\,\text{N/m}^2$, $C_{44} = 2.56 \times 10^{10}\,\text{N/m}^2$, $f_{15} = 12.7\text{C/m}^2$,

$f_{31} = -5.2\text{C/m}^2$, $f_{33} = 15.1\text{C/m}^2$, $\zeta_{11} = 650 \times 10^{-11}\,\text{F/m}$, $\zeta_{33} = 560 \times 10^{-11}\,\text{F/m}$,

$\rho = 7500\text{kg/m}^3$,

for ZnO

$C_{11} = 20.97 \times 10^{10}\,\text{N/m}^2$, $C_{12} = 12.11 \times 10^{10}\,\text{N/m}^2$, $C_{13} = 10.51 \times 10^{10}\,\text{N/m}^2$,

$C_{33} = 21.09 \times 10^{10}\,\text{N/m}^2$, $C_{44} = 4.25 \times 10^{10}\,\text{N/m}^2$, $f_{15} = -0.59\text{C/m}^2$,

$f_{31} = -0.61\text{C/m}^2$, $f_{33} = 1.14\text{C/m}^2$, $\zeta_{11} = 7.38 \times 10^{-11}\,\text{F/m}$, $\zeta_{33} = 7.83 \times 10^{-11}\,\text{F/m}$,

$\rho = 5676\text{kg/m}^3$,

and for epoxy-resin

$\lambda^e = 42.31\times10^9\,\mathrm{N/m^2}$, $\mu^e = 3.76\times10^9\,\mathrm{N/m^2}$, $A^e = 2.8\times10^9\,\mathrm{N/m^2}$, $B^e = 9.7\times10^9\,\mathrm{N/m^2}$, $C^e = -5.7\times10^9\,\mathrm{N/m^2}$, and $\rho^e = 1170\,\mathrm{kg/m^3}$.

The independent sets of equations (36) yield two independent classes of free vibrations [14]. The first class does not involve the piezoelectric or dielectric parameters, being identical to the one for the corresponding spherically isotropic elastic sphere. The second class depends on the piezoelectric or dielectric parameters. With the increase of the gradient index λ, the natural frequencies increase for all modes and functionally graded laws, the variation being more significant when $\lambda \le 10$. For $\lambda \to \infty$ the variation of natural frequencies is not significant with respect to those of $\lambda = 10$. It is seen that for a piezoceramic hollow sphere, the piezoelectric effect consists in increasing the values for the natural frequencies in both classes of vibrations. If $\xi = 2r/a$ increases, the natural frequencies increase for the first class of vibrations and decrease for the second class.

We have compared different boundary conditions to test the effectiveness of non-reflecting boundary conditions implemented in the simulation. The output of the coupled modes is compared with the input waves, as shown in Fig. 2, in the case of Reddy law for $\lambda = 10$. We see that the ratio of the coupled and input waves is −3 to −18 dB around the frequency of 8kHz to 8.8kHz in the band-gap of the sonic material.

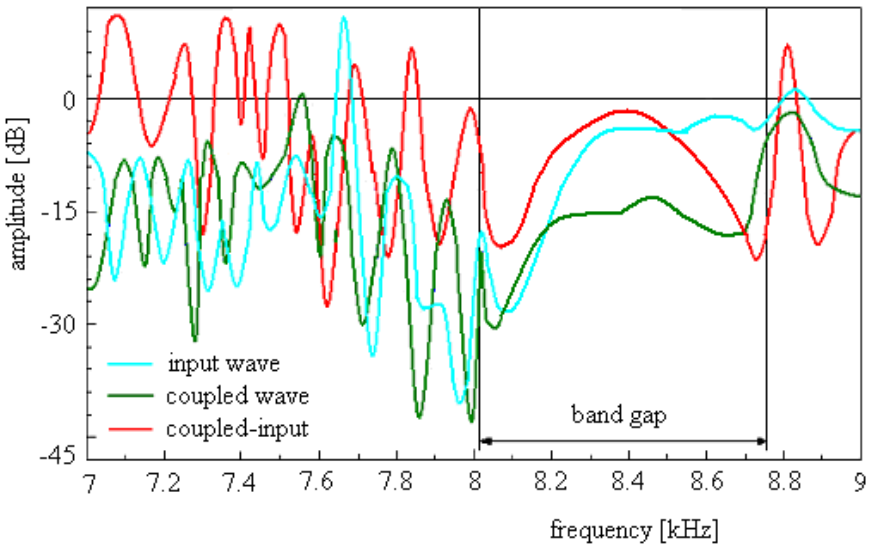

Fig. 2. Input and coupled waves for sonic composite in the case of Reddy law for $\lambda = 10$.

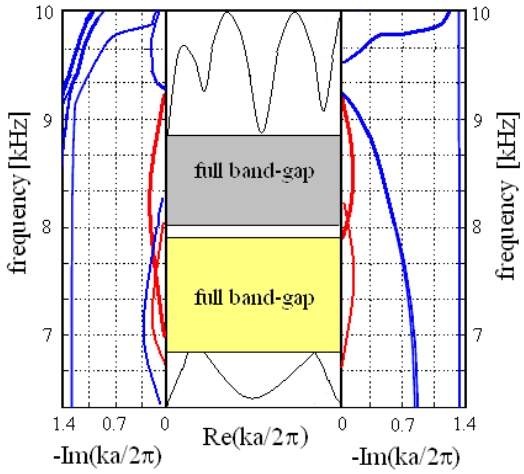

Fig. 3. Band structure for the sonic composite in the case of Reddy law for $\lambda = 10$ (grey) and $\lambda = 5$ (yellow).

The effect of the gradient index λ on the full band-gap size is studied next. The size variation is clearly observed for $\lambda \leq 10$, while for $\lambda \to \infty$ the changes are not significant.

Using the Joannopoulus representation for the band-gap structure with the evanescent modes having exponential decay, Fig. 3. displays the band structure for $\lambda = 5$ (yellow) and $\lambda = 10$ (grey) ($\xi_0 = 0.3$). The modes present purely imaginary wave vectors. The central grey region is the full band-gap given by the real part of the wave vector constrained in the first Brillouin zone for each frequency. The left region represents the imaginary part of the wave vector for longitudinal direction frequency (tension/compression), while the right region is the imaginary part of the wave vector for transverse direction frequency (shear). The red lines represent the imaginary part of the wave vector of the evanescent modes inside the bad-gap. If we want to have a full band-gap, we must have structures with band-gaps for both longitudinal and transverse waves in the same frequency region. The full band-gap has different lengths and frequency locations for different values of $\lambda \leq 10$. The numerical investigations show us that a maximum size of the full band is obtained in the vicinity of $\lambda = 9.7$. In this case the full band-gap is higher than in the case of $\lambda = 10$ with 7%.

Finally we consider now a real sonic composite, namely the sonic-crystal bulk of acrylic resin rods in air [19, 20].

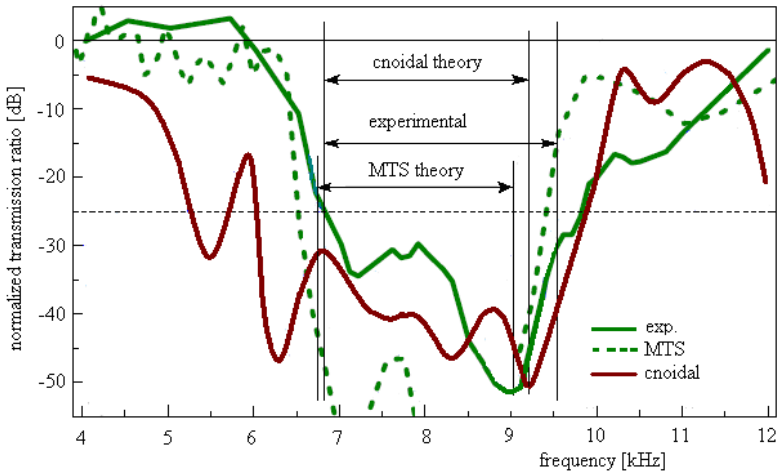

Fig. 4. The band-gap structures of a sonic crystal of acrylic resin rods in air.

The materials considered are the acrylic resin. The lattice constant is 24.0 mm, the radius of the scatterers is 10.2 mm and their length is approximately 30 cm. Both the top and the bottom sides have sufficient amounts of glass wool to effectively absorb the sound waves of oblique wave fronts. A straight wave-guide, as well as a bending wave-guide, was constructed in this sonic-crystal bulk. The experimental results show a clear and deep full band-gap in the transmission spectra, as illustrated with continuous green line in Fig. 4. The measured full band-gap was 6.8–9.5 kHz, or 0.475–0.67 in normalized frequencies with a transmission ratio smaller than −25 dB. The experimental band-gap is 20% wider than the theoretical result of Miyashita, Taniguchi and Sakamoto (MTS) [19]. In the MTS analysis, the wave propagation is simulated by finite element method with the open-space conditions normally encountered. We see that the experimental band-gap is 8% wider than the theoretical result obtained by the method proposed in this paper.

4. Conclusions

The cnoidal method combined with the piezoceramic theory was implemented in this paper for simulating and analysing the behaviour of a sonic plate with an array of acoustic piezoceramic hollow spheres embedded in an epoxy matrix. The scatterers are made from functionally graded materials with radial polarization. The influence of the gradient index of the Reddy material on the full band-gap size is studied using the cnoidal representations of the solutions.

Finally, a real sonic-crystal bulk of acrylic resin rods in air has been analyzed to validate the theory. The present method can be further extended to investigate other sonic composites with different types of scatterers embedded in arbitrary, homogeneous media.

Acknowledgement

The authors gratefully acknowledge the financial support of the National Authority for Scientific Research ANCS/UEFISCDI through the project PN-II-ID-PCE-2012-4-0023, Contract nr.3/2013. This work was elaborated during the doctoral studies of PhD student Ruxandra Ilie.

REFERENCES

[1]. *A. R. Osborne,* Soliton physics and the periodic inverse scattering transform, Physica D 86, 1995, pp. 81-89.
[2]. *G. Drazin, R. S. Johnson*, Solitons. An Introduction, Cambridge Univ. Press, 1989.
[3]. *M. J. Ablowitz, H. Segur,* Solitons and the Inverse Scattering Transforms, SIAM, Philadelphia, 1981.
[4]. *M. J. Ablowitz, P.A. Clarkso*, Solitons, Nonlinear Evolution Equations and Inverse Scattering, Cambridge Univ. Press, Cambridge, 1991.
[5]. *L. Munteanu, St. Donescu,* Introduction to Soliton Theory: Applications to Mechanics, Book Series Fundamental Theories of Physics, Kluwer Academic Publishers, Dordrecht, Boston (Springer Netherlands), **vol.143**, 2004.
[6]. *B. A. Dubrovin, V. B. Matveev, S. P. Novikov,* Nonlinear equations of Korteweg-de Vries type, finite zone linear operators, and Abelian varietes, Russ. Math. Surv., 31(1), 1976, pp. 59-146.
[7]. *M. Abramowitz, I. A. Stegun*, (eds.), Handbook of mathematical functions, U. S. Dept. of Commerce, 1984.
[8]. *W. Magnus, R. Oberhettinger, P. Soni*, Formulas and Theorems for the Special Functions of Mathematical Physics, Springer, New York, 1966.
[9]. *L. Munteanu, V. Chiroiu*, On the dynamics of locally resonant sonic composites, European Journal of Mechanics-A/Solids, 29(5), 2010, pp. 871–878.
[10]]. *L. Munteanu, V. Chiroiu, St. Donescu, C. Brişan*, A new class of sonic composites, Journal of Applied Physics, 115, 104904, 2014.
[11]. *V. Chiroiu, C. Brişan, M. A. Popescu, I. Girip, L. Munteanu*, On the sonic composites without/with defects, Journal of Applied Physics, 114(16), 164909-1-10, 2013.
[12]. *J. N. Reddy*, A Generalization of Two-Dimensional Theories of Laminated Composite Laminate, Comm. Appl. Numer. Meth.,, 3,1987, pp. 173–180.
[13]. *J. N. Reddy, C. M. Wang, S. Kitipornchai*, Axisymmetric bending of functionally graded circular and annular plates, Eur. J. Mech., A/Solids, 18, 1999, pp. 185–199.
[14]. *V. Chiroiu, L. Munteanu*, On the free vibrations of a piezoceramic hollow sphere, Mech. Res. Comm., Elsevier, 34, 2, 2007, pp. 123–129.
[15]. *W. Q. Chen, L. Z. Wang, Y. Lu*, Free vibrations of functionally graded piezoceramic hollow spheres with radial polarization, J. Sound Vibr., 251, 1, 2002, pp. 103–114.
[16]. *R. A. Toupin*, Piezoelectric relations and the radial deformation of a polarized spherical shell, J. Acoust. Soc. Am., 31, 1959, pp. 315–318.
[17]. *E. Dieulesaint, D. Royer*, Elastic waves in solids, New York, John Wiley, 1980.
[18]. *Y. Y. Tang, K. Xu*, Exact solutions of piezoelectric materials with moving screw and edge dislocation, Int. J. Eng. Sci., 32, 1994, pp. 1579–1591.
[19]. *T. Miyashita, R. Taniguchi, H. Sakamoto*, Experimental full band-gap of a sonic-crystal slab structure of a 2D lattice of aluminum rods in air, Proc. 5th World Congress on Ultrasonics TO-PM04.02, 2003.
[20]. *T. Miyashita*, Full band gaps of sonic crystals made of acrylic cylinders in air-numerical and experimental investigations, Jpn. J. Appl. Phys. 41, 3170-1-3175, 2002.